Compression Field Analysis of Fiber-Reinforced Concrete Based on Cracked Membrane Model

Author(s):
Kaufmann, Walter; Mata Falcón, Jaime; Amin, Ali

Publication date:
2019-09

Permanent link:
https://doi.org/10.3929/ethz-b-000365523

Originally published in:
ACI Structural Journal 116(5), https://doi.org/10.14359/51716763

COMPRESSION FIELD ANALYSIS OF FRC BASED ON THE CRACKED MEMBRANE MODEL

Walter Kaufmann, Jaime Mata-Falcón and Ali Amin

BIOGRAPHY

Walter Kaufmann is Professor and Chair of Concrete Structures and Bridge Design at ETH Zurich, Switzerland. He has over 25 years of experience working both in academia and as a structural engineer. His research interests include the design and analysis of conventional, prestressed, digitally fabricated, and fiber-reinforced concrete structures.

Jaime Mata-Falcón is a Postdoctoral Researcher at ETH Zurich, Switzerland. He received his Master's and PhD degrees from the Polytechnic University of Valencia, Spain. His research interests include the design and analysis of conventionally and digitally fabricated concrete structures.

Ali Amin is a Lecturer in the School of Civil Engineering at The University of Sydney, Australia. He received his BE and PhD from UNSW Australia in 2011 and 2015, respectively. He is a member of the Concrete Institute of Australia. His research interests include the structural design and analysis of fiber reinforced and high performance concretes.

ABSTRACT

Compression field approaches are well established methods used to analyze the load-deformation behavior of reinforced concrete elements subjected to in-plane shear and normal forces. In this paper, the simplified Cracked Membrane Model considering rotating, stress-free cracks is extended to include the effect of fiber reinforcement. The key advantage of the proposed compression field approach is that it yields the most important factors for the design and analysis of fiber reinforced concrete (FRC) – that is, crack opening and spacing – directly. A solution procedure is developed herein for two practical design cases for webs of girders without conventional shear reinforcement. In both cases, the applied load can typically be increased after cracking even when using strain softening FRC. The model is shown to predict the response of available test data on uniaxially

reinforced FRC panels satisfactorily but fails to capture failures governed by sliding of cracks in elements containing high fiber dosages.

Keywords: fiber reinforced concrete; in-plane shear and normal forces; plane stress; compression field approaches; shear strength; load-deformation analysis.

INTRODUCTION

It is widely recognized in academia and practice that the addition of steel fibers to concrete may significantly increase the shear strength of reinforced concrete. In certain cases, steel fibers have the capacity to completely replace conventional shear ligature reinforcement[1]. This is particularly appealing from an economic and architectural perspective, as the replacement of manually placed steel bar reinforcement with an equivalent dosage of fiber reinforced concrete (FRC) would be extremely beneficial to a project's construction speed, and eliminating the installation of conventional reinforcement would facilitate the construction of free form, non-orthogonal beam and slab geometries, which may otherwise be difficult with conventional reinforcing bar layouts and formwork systems.

However, using practical and economical fiber dosages, FRC typically exhibits a softening response in tension after cracking has occurred. Such behavior at the material constitutive level has the potential to lead to a localization of the deformations in single cracks. On the other hand, classical design philosophy in structural concrete relies on members displaying strain hardening behavior in order to achieve a sufficient amount of ductility, which is required to enable the imposed actions to redistribute as the collapse load is approached. This is a prerequisite for the omission of restraint stresses caused by imposed deformations, restrained shrinkage and thermal contraction after hydration etc. in ultimate limit state design. Hence, designers are justifiably hesitant to use FRC without a substantial amount of additional conventional longitudinal steel reinforcement for structural members. Design codes such as AS3600-2018[2] have imposed severe limits on the use of FRC for such purposes. This reluctance of using fiber only solutions is certainly justified for elements stressed

in tension, where the addition of moderate amounts of fibers may even have a detrimental effect on the ductility of girders containing conventional longitudinal reinforcing steels[3,4]. However, it is less understandable for elements subjected to shear, where conventionally reinforced concrete girders, in compliance with international design codes, usually contain transverse reinforcement ratios in the order of about one quarter of the amount required to achieve a ductile behavior in tension (see References[5,6]). In fact, many experimental campaigns[7–11] have shown that this is sufficient to avoid premature, brittle shear failures, even if activating the shear resistance requires substantial stress redistribution in the web. Furthermore, several experimental studies on the shear behavior of FRC beams[12–15] indicate that brittle shear failures can be mitigated and transformed to ductile flexural failures by adding a sufficient dosage of steel fibers to the concrete, without providing additional conventional transverse stirrup reinforcement.

Indeed, several recently revised international codes of practice now contain provisions, which permit designers to rely on steel fibers in carrying a portion of the imposed one-way shear in structural concrete[2,16–18]. However, the conditions for such applications are restrictive, typically limiting the use of steel fibers to resist relatively low shear forces (e.g. 30% of the total shear according to Reference[16]) and requiring uneconomically high minimum fiber contents (e.g. $\rho_{f,\min} = 0.75\%$ according to ACI-318[18]) which may impede the workability of fresh concrete. Such severe restrictions for the use of steel fibers as the only mechanism in carrying shear in structural concrete are pertinent and should be respected, as long as existing models for the global shear strength of fiber reinforced concrete members are semi-empirical. Generally, these design approaches assume that the total shear V_R, is partially resisted by a component taken by the plain concrete, V_{Rc}, a component taken by the fibers, V_{Rf}, and, where applicable, a component resisted by the transverse reinforcement, V_{Rs}, resulting in a total resistance $V_R = V_{Rc} + V_{Rf} + V_{Rs}$. The V_{Rs} component is usually obtained from a truss model and the components V_{Rc} and V_{Rf} are typically calibrated on tests. A first step in the direction of a mechanically based model for the shear strength of FRC was made by the alternative approach mentioned in the explanations to the *fib* Model Code 2010[19–21], which includes a fiber contribution

V_{Rf} that essentially corresponds to a compression field approach. However, the inclination of the compression field and the crack width required in determining the effective fiber bridging stresses are evaluated using semi-empirical equations. Furthermore, the empirical concrete contribution, V_{Rc}, which is somewhat related to the shear at the commencement of diagonal cracking, is still added to obtain the global shear strength. This is in contrast to well-established approaches for conventionally reinforced structural concrete, where if the minimum shear reinforcement discussed above is provided, a safe and economical design is possible using a simple variable angle truss model approach, based on the lower bound theorem of the theory of plasticity[19,22,23], without the need for empirical concrete contributions. In order to fully exploit the potential of using steel fibers as shear reinforcement, mechanically consistent models for the design and analysis of FRC in shear must be developed.

RESEARCH SIGNIFICANCE

It is well established that the addition of fibers to concrete increases the shear strength of a reinforced concrete member. Available models describing the behavior of fiber reinforced concrete (FRC) in shear are, however, founded on semi-empirical rationale. This paper presents a mechanically consistent rotating crack model to describe the behavior of FRC elements in plane stress. The model is based on the Cracked Membrane Model[23,24], a compression field approach for conventionally reinforced concrete, extended herein to account for fiber reinforcement. Through this study, improved methods of analysis of FRC members subjected to shear can be rationally achieved.

COMPRESSION FIELD APPROACHES

Compression field approaches for conventionally reinforced concrete elements

The load-deformation behavior of diagonally cracked reinforced concrete elements can be readily analyzed using compression-field approaches. These approaches were developed several decades ago[25,26], and systematically satisfy equilibrium conditions and compatibility requirements. The basic concepts of such models are illustrated in Fig. 1 for the special case of orthogonal reinforcement,

whereby the horizontal and vertical reinforcement are assumed to coincide with the *x*- and *z*-directions, respectively.

Consider the element shown in Fig. 1a. Noting that the sum of forces in the concrete and reinforcement must correspond to the applied loads (Fig. 1d), the following two equivalent sets of equilibrium conditions are obtained

$$\begin{aligned} \sigma_x &= \sigma_{cx} + \sigma_{sx} = \sigma_{c3}\cos^2\theta + \sigma_{c1}\sin^2\theta + \rho_x\sigma_{sx} \\ \sigma_z &= \sigma_{cz} + \sigma_{sz} = \sigma_{c3}\sin^2\theta + \sigma_{c1}\cos^2\theta + \rho_z\sigma_{sz} \\ \tau_{zx} &= \tau_{czx} + \tau_{szx} = (\sigma_{c1} - \sigma_{c3})\sin\theta\cos\theta \end{aligned} \quad \text{or} \quad \begin{aligned} \rho_x\sigma_{sx} &= \sigma_x + \tau_{zx}\cot\theta - \sigma_{c1} \\ \rho_z\sigma_{sz} &= \sigma_z + \tau_{zx}\tan\theta - \sigma_{c1} \\ \sigma_{c3} &= -\tau_{zx}(\tan\theta + \cot\theta) + \sigma_{c1} \end{aligned} \tag{1}$$

if the reinforcing bars are assumed to only carry uniaxial stresses along their longitudinal axis, i.e. neglecting dowel action such that $\tau_{szx} = 0$. In Fig. 1d, ρ_x and ρ_z are the geometric reinforcement ratios in the *x*- and *z*-directions, respectively, σ_c and σ_s are the stresses in the concrete and reinforcement, respectively and θ is the principal compressive stress and strain direction. Compatibility requires that the strains (Fig. 1b) are related through

$$\cot^2\theta = \frac{\varepsilon_z - \varepsilon_3}{\varepsilon_x - \varepsilon_3} = \frac{\varepsilon_1 - \varepsilon_x}{\varepsilon_x - \varepsilon_3} = \frac{\varepsilon_z - \varepsilon_3}{\varepsilon_1 - \varepsilon_z} \tag{2}$$

i.e., the state of strain is fully determined by three independent unknowns. Expressing the concrete stresses (σ_{c1}, σ_{c3}) and the stresses in the reinforcement (σ_{sx}, σ_{sz}) in terms of any 3 non-collinear strains, e.g. ($\varepsilon_x, \varepsilon_z, \varepsilon_3$), and using constitutive relationships relating stresses and strains of concrete and reinforcement, respectively, the states of stress and strain can be determined iteratively by solving the 3 equations in Eqs. (1) for the 3 unknown strains.

The Equations presented in Eqs. (1) may be simplified by neglecting the tensile stresses in the concrete (i.e. $\sigma_{c1} = 0$, refer to Fig. 1c), as typically assumed in design[23]. For linear elastic behavior for the reinforcement and concrete, with $n = E_s/E_c$, Baumann's closed-form equation for the principal compressive stress and strain direction is obtained[27]:

$$\tan^2\theta\rho_x(1 + n\rho_z) + \tan\theta\rho_x\frac{\sigma_z}{\tau_{xz}} = \cot^2\theta\rho_z(1 + n\rho_x) + \cot\theta\rho_z\frac{\sigma_x}{\tau_{xz}} \tag{3}$$

Having determined the principal compressive stress and strain direction θ from Eq. (3), obtaining the response (strains for any given applied stresses) by inserting θ in Eqs. (1) is straightforward.

Neglecting the tensile strength of the concrete, f_{ct}, in any direction corresponds to the assumption of fictitious, rotating, stress-free cracks which open orthogonally, and hence, the principal compressive directions of average strains θ_ε and concrete stresses θ_σ coincide with the direction of the fictitious cracks θ_r ($\theta_r = \theta_\varepsilon = \theta_\sigma = \theta$), refer to Fig. 1. Predictions obtained using this type of classical compression field approach – even if using nonlinear constitutive relationships for concrete and reinforcement[28] – tend to overestimate the observed deformations since rotating cracks are considered and tension stiffening effects are neglected. Furthermore, they typically overestimate the ultimate load unless compression softening of the concrete is accounted for[23].

Vecchio and Collins proposed the Modified Compression Field Theory (MCFT)[29] to overcome these weaknesses. In the MCFT, tension stiffening is implicitly taken into account by formulating equilibrium in terms of average stresses between the cracks, including average tensile stresses in the concrete (Fig. 1d). However, by treating the assumed average tensile stresses in the concrete as a material property, depending only on the principal tensile strain, the respective empirical constitutive equations disregard the fact that tension stiffening strongly depends on the rebar diameter and the steel reinforcement ratios[30]. Consequently, such an approach is unable to yield direct information on the maximum stresses at the cracks nor on crack spacings or crack widths. The same remark applies to other models formulating equilibrium in terms of average stresses between cracks[31,32].

Extending this methodology for FRC is not entirely appropriate as the most important property when considering the design of a structural member manufactured with FRC is its post cracking, or residual, tensile strength. The strength that is offered by the fibers across a crack is dependent on the width of the crack. Hence for a reliable analysis of FRC elements, information on the crack opening must be established. This is why compression field models formulating equilibrium in terms of stresses at the cracks, which can yield direct information on crack spacing and openings, are much better suited for the analysis of FRC elements in shear. One such model is the Cracked Membrane Model (CMM)[23,24].

In its general formulation (CMM-F), this model allows treating cracks as fixed and interlocked rather than as rotating and stress-free while accounting for shear and normal stresses on the crack faces as well as bond stresses transferred between the concrete and steel reinforcement. Equilibrium conditions are expressed in terms of stresses at the cracks (see Fig. 2), and crack spacings and tensile stresses between the cracks are determined from basic mechanical principles adopted from the Tension Chord Model (TCM)[5]. However, calculations using this general model are tedious, and the assumption of interlocked cracks with a fixed direction is of limited use for design purposes, since this is equivalent to allowing substantial tensile stresses to develop in the concrete between the cracks. Therefore, the simplified version of the model considering rotating, stress-free cracks, the CMM-R, is considered in the following[23,24]. This model has been successfully implemented in FE-codes by several researchers[33–35], including a generalization to the analysis of shell elements using a sandwich model approach[36–38].

In the CMM-R, contrary to the CMM-F, cracks are assumed to be stress free and open orthogonally. These two assumptions greatly simplify the calculations without losing the direct information on the local stresses at the cracks and crack openings, since equilibrium conditions are expressed in terms of stresses at the cracks. In particular, Eqs. (1) can be simplified neglecting the tensile stresses in the concrete at the cracks (i.e. setting $\sigma_{c1} = 0,$ refer to Fig. 1c) and remain valid if stresses in the concrete and reinforcement at the cracks, as well as $\theta_r = \theta$ are inserted, and a closed form solution for the diagonal crack spacing, s_r, can be established based on the theoretical maximum crack spacings for uniaxial tension in the reinforcement directions, s_{rx0} and s_{rz0}, respectively[23,24]. The latter are obtained observing that while $\sigma_{c1} = 0$ at the cracks, tensile stresses are transferred to the concrete between the cracks by bond shear stresses, and that the tensile stresses in the concrete cannot exceed f_{ct} midway between two cracks. Using the TCM[5], which assumes constant rigid-plastic bond stresses (i.e. independent of the slip) prior to yielding of the reinforcement, the maximum theoretical crack spacings for uniaxial tension are given by

$$s_{rx0} = \frac{\varnothing_x f_{ct}(1-\rho_x)}{2\tau_{b0}\rho_x} \approx \frac{\varnothing_x f_{ct}}{2\tau_{b0}\rho_x} = \frac{\varnothing_x}{4\rho_x},\ s_{rz0} = \frac{\varnothing_z f_{ct}(1-\rho_z)}{2\tau_{b0}\rho_z} \approx \frac{\varnothing_z}{4\rho_z} \qquad (\tau_{b0} = 2f_{ct}) \tag{4}$$

where $\varnothing_x$ and $\varnothing_z$ are the bar diameters in the *x*- and *z*-directions, respectively, $\tau_{b0} = 2f_{ct} = 0.6f_c^{2/3}$ is the bond shear stress for elastic reinforcement according to the TCM, with f_c being the concrete cylinder strength in MPa units. Note that the minimum theoretical crack spacing is half the corresponding maximum crack spacing, since at the limit, a new crack may form when $\sigma_{c1} = f_{ct}$ is attained midway between two cracks. This uncertainty cannot be avoided, even with more realistic, complex bond shear stress-slip relationships, which justifies the use of a simplified, yet mechanically consistent model like the TCM[5]. In order to determine the crack spacing in biaxially reinforced elements, the stresses in the concrete between the cracks can be determined by superimposing the concrete stresses at the crack with the stresses transferred to the concrete between the cracks by bond shear stresses from both sets of orthogonally placed reinforcing bars. Noting that the crack spacings are geometrically related through $s_r = s_{rx}\sin\theta = s_{rz}\cos\theta$ (see Fig. 2a), and that just as for uniaxial tension, the maximum diagonal crack spacing s_{r0} is attained when $\sigma_{c1} = f_{ct}$ occurs at the center between two cracks, s_{r0} can be determined analytically[23,24]. A good upper bound approximation for s_{r0} is given by

$$s_{r0} = \frac{1}{\frac{\sin\theta}{s_{rx0}} + \frac{\cos\theta}{s_{rz0}}} \tag{5}$$

Eq. (5) is the same equation postulated by Vecchio and Collins[29]. Like in uniaxial tension[5,6], the diagonal crack spacing may also vary by a factor of two, i.e. $s_r = \lambda s_{r0}$, with $\lambda = 0.5\ldots1.0$ [23,24]. The crack opening, w_r, can be determined from the principal tensile strain, ε_1, and the diagonal crack spacing $s_r = \lambda s_{r0}$, i.e.

$$w_r = s_r(\varepsilon_1 - \varepsilon_{c1}) \approx s_r\varepsilon_1 = \lambda s_{r0}\varepsilon_1 \tag{6}$$

196 Eq. (6) is simplified by neglecting the tensile strains within the concrete between the cracks, ε_{c1},

197 without significantly affecting accuracy, since typically, $\varepsilon_{c1} \ll \varepsilon_1$.

198 Knowing the crack spacing (or rather, selecting a value between its theoretical upper and lower
199 boundaries), the CMM-R analysis can be carried out as outlined above for classic compression field
200 models, i.e. solving the Eqs. (1) (with $\sigma_{c1} = 0$) to obtain the state of strain (3 unknowns) for any given
201 set of applied stresses. However, constitutive relationships for the concrete and the reinforcement
202 expressing the (maximum) stresses at the cracks in terms of average strains are required. The TCM
203 allows for determining these relationships consistently as a function of the crack spacing[5], with
204 closed-form analytical solutions e.g. when using a bilinear stress-strain relationship for the bare bar
205 reinforcement. For linear elastic reinforcement, a closed form solution for the crack inclination θ_r,
206 similar to Eq. (3) but accounting for tension stiffening in a consistent manner, can be derived, and is
207 a useful tool for verifications of the serviceability limit state, particularly for crack widths[39]. For more
208 details, the reader is referred to References[23,24].

209 **Compression field approach for FRC elements**

210 Adapting the CMM-R to account for fiber reinforcement (CMM-Rf) is straightforward, since
211 equilibrium is formulated at the cracks and fiber stresses at cracks can be determined from the crack
212 kinematics that are directly obtained from the model. Hence, equilibrium can simply be expressed
213 using Eqs. (1) (Fig. 1d), and setting $\sigma_{c1} = \sigma_{cf}$, where σ_{cf} is the effective (residual) fiber stresses at
214 the cracks. These stresses act perpendicularly to the crack face and hence, in the direction of the
215 principal concrete tensile stresses. The residual stresses provided by the fibers are dependent on the
216 crack opening, i.e. $\sigma_{c1} = \sigma_{cf}(u)$, where $u = w_r$ and can be obtained from Eq. (6).

217 However, the crack spacings (refer to Eq. (4)) need to be adapted to account for the fiber bridging
218 stresses. As outlined above for conventional reinforced concrete, moving away from a crack along a
219 reinforcing bar, the tensile stresses in the surrounding concrete will gradually build up, as a result of
220 bond shear stresses transferred from the reinforcement, to a value up to f_{ct}. This distance is shorter in

221 FRC than in concrete without fibers since in addition to bond, the fiber stresses $\sigma_{c1} = \sigma_{cf}$ at the crack
222 are transmitted to the concrete over the fiber embedment length $l_{bf} \le l_f/2$. Using the same
223 assumptions as in the TCM, the following crack spacings for uniaxial tension in the reinforcement
224 directions, accounting for additional fiber reinforcement, result[3]:

225 $$s_{rxf0} = \frac{Ø_x}{4\rho_x}\left(1 - \frac{\sigma_{cf}}{f_{ct}}\right),\ s_{rzf0} = \frac{Ø_z}{4\rho_z}\left(1 - \frac{\sigma_{cf}}{f_{ct}}\right) \qquad \left(\tau_{b0} = 2f_{ct}\right) \tag{7}$$

226 Using Eqs. (7), the maximum diagonal crack spacing can be determined as for conventionally
227 reinforced panels, again with $s_{rf} = \lambda s_{rf0}$ ($\lambda = 0.5 \ldots 1.0$)[23,24]. The diagonal crack spacing
228 $s_{rf} = s_{rzf}\sin\theta = s_{rxf}\cos\theta$ accounting for biaxial reinforcement and fibers, can be determined based on
229 the theoretical maximum diagonal crack spacing, s_{rf0}, as follows:

230 $$s_{rf0} = \frac{1}{\frac{\sin\theta}{s_{rxf0}} + \frac{\cos\theta}{s_{rzf0}}} = \frac{1 - \sigma_{cf}/f_{ct}}{\frac{\sin\theta}{s_{rx0}} + \frac{\cos\theta}{s_{rz0}}},\quad s_{rf} = (0.5 \ldots 1.0)s_{rf0} \ge l_f \tag{8}$$

231 where θ is the principal compressive stress direction at the onset of initial cracking.
232 Note that for high fiber dosages, Eqs. (7) can yield very small or even negative crack spacings (for
233 $\sigma_{cf} > f_{ct}$); however, this is physically impossible since for small crack spacings, these high fiber
234 stresses cannot be activated. By this, an imposed lower bound limit for the crack spacing is taken as
235 the length of the fiber (i.e. $s_{rf} \ge l_f$) as indicated in Eq. (8). Since the crack opening is typically small
236 during the crack formation process, a reasonable approximation of the crack spacing is obtained by
237 setting $\sigma_{cf} \approx \sigma_{cf0}$ in Eqs. (7) and (8), where σ_{cf0} denotes the fiber effectiveness, corresponding to
238 the maximum value of residual fiber stresses at small crack openings as further outlined below (refer
239 to Eq. (11)).
240 For members without conventional reinforcement in either direction, Eq. (8) cannot be used. Rather,
241 for members with high fiber dosages, the crack spacing will be in the order of $s_{rf} \approx l_f$, and for low
242 fiber dosages, localized cracking is expected to occur unless the crack spacing in either direction is

243 governed by adjacent elements, such as the chords in the case of the web of a girder. In the latter case,
244 the diagonal crack spacing in the web can be estimated geometrically, using the crack spacing $s_{rx,TC}$
245 in the tension chord:

246 $$s_{rf} = s_{rx,TC} \sin\theta \tag{9}$$

247 Knowing the crack spacing, the value of σ_{cf} can be determined for a given state of strain (and hence
248 crack opening) using Eq. (6) and any suitable FRC material constitutive stress vs crack opening
249 relationship. In this paper, the simple mechanical model proposed by Pfyl[3,40], illustrated in Fig. 3, is
250 adopted to estimate the residual characteristics of the FRC for the sake of simplicity. It is
251 acknowledged that more accurate expressions for the residual capacity of FRC may be obtained using
252 fiber stress vs crack opening characteristics derived directly from standard material tests on the actual
253 FRC used[41], or through the use of more refined/sophisticated constitutive models that are available in
254 the literature[42,43]. Also, better predictions are likely to be obtained using statistical models to predict
255 material parameters; however, this is beyond the scope of this paper.
256 While Pfyl's model considers fiber activation followed by a pull-out phase, only the latter is
257 considered in the following for simplicity (Fig. 3b). Hence, fiber stresses amount to

258 $$\frac{\sigma_{cf}}{\sigma_{cf0}} = \left(1 - \frac{2u}{l_f}\right)^2 \qquad \left(u \le \frac{l_f}{2}\right) \tag{10}$$

259 In the derivation of Eq. (10), fiber snubbing effects[43] were neglected. The term σ_{cf0} denotes the *fiber*
260 *effectiveness* of the FRC, which can be expressed as

261 $$\sigma_{cf0} = K_f \frac{\rho_f \tau_{bf} l_f}{d_f} \tag{11}$$

262 if the pullout resistance of the individual fibers is assumed to be independent of their inclination θ_f
263 with respect to the outer normal to the crack surface. This assumption can be justified if fibers oriented
264 close to the crack plane (e.g. $\theta_f > \pi/3$ as proposed by Foster[44]) are considered ineffective, as
265 assumed in the following. In Eq. (11), ρ_f is the total volumetric fiber content, K_f is a fiber

orientation factor explained in the Appendix, and τ_{bf} is the average bond stress between the fibers and surrounding matrix along the shorter embedded length, which accounts for stress transfer between the fibers and the matrix by anchorage provided by end hooks, taken as $\tau_{bf} = 2 f_{ct} = 0.6 f_c^{2/3}$ (in MPa units).

In the discussion above a fundamental assumption is made on the failure mechanism of FRC in that the fibers pull-out of the matrix. If the axial stresses developed within the fibers exceeded the ultimate tensile strength of the fibers, f_{tf}, the fibers would fracture before being pulled out. Pfyl's model above can be extended for the case of fiber fracture, noting that fibers longer than

$$l_{fbu} = \frac{f_{tf} d_f}{4\tau_{bf}} \tag{12}$$

would fracture before completely pulling out. However, the fiber geometry (l_f, d_f) and properties are usually tuned to avoid this behavior. Therefore, fiber fracture is not considered in the development of the model.

Furthermore, it has been observed in tests on FRC members where single dominant/localized cracks form that the number of fibers bridging failure surfaces are generally lower than the total expected number of fibers[41]. It is thought that the crack path follows the easiest propagation route through the FRC matrix and often propagates through the inherent flaws of the concrete (such as pores) and near the end or around individual fibers. In shear critical FRC beams, Amin and Foster[45] included a fiber dispersion factor of 0.82 which is applied to the average residual tension that is offered by the fibers to account for these observations. For FRC members containing steel rebar where many cracks are expected to form, it may be argued that the initial cracks may contain, on average, fewer fibers than theoretically expected. However, after first cracking, the location of the subsequent cracks depends more-so on the development of bond between the FRC matrix and steel rebar than the presence of the fibers. Assuming many cracks smeared along the element, and large crack surfaces, the influence of those few initial cracks with statistically fewer fibers becomes negligible to the overall response of

290 the element. Note that it has also been observed in tension tie tests that one of these initial cracks is
291 more likely to develop into the failure surface of the member, however these failure surfaces tend to
292 localize well after peak load has been attained[46,47].
293 The CMM-Rf analysis including fibers can be carried out just as outlined above for the CMM-R
294 without fibers, but solving Eq. (1) with $\sigma_{c1} = \sigma_{cf}(u)$ instead with $\sigma_{c1} = 0$ to obtain the state of strain
295 (3 unknowns) for a given set of applied stresses, where the crack opening $u = w_r$ can be determined
296 from Eq. (6), using the crack spacing given by Eq. (8).
297 **Simplified compression field approach for FRC webs**
298 For elements without vertical reinforcement nor vertically applied stresses, as is the case for the webs
299 of girders without conventional shear stirrup reinforcement, the compression field analysis presented
300 above can be simplified. Using Eqs. (1) with $\sigma_{c1} = \sigma_{cf}$ and setting $\rho_z = \sigma_z = 0$, one obtains (Fig. 4c)

$$\rho_x \sigma_{sx} - \sigma_x = \tau_{zx} \cot\theta - \sigma_{cf} = \tau_{zx}\left(\frac{\tau_{zx}}{\sigma_{cf}} - \frac{\sigma_{cf}}{\tau_{zx}}\right) = \frac{\tau_{zx}^2}{\sigma_{cf}} - \sigma_{cf}$$

301 $$\tan\theta = \frac{\sigma_{cf}}{\tau_{zx}} \qquad (13)$$

$$\sigma_{c3} = -\frac{\tau_{zx}^2}{\sigma_{cf}}$$

302 Knowing σ_{cf}, the state of stress at the cracks for any applied stresses (σ_x, τ_{zx}) is thus uniquely
303 determined by equilibrium alone. However, σ_{cf} is a function of the crack opening, which in turn is
304 dependent on the principal tensile strain (see Eq. (6)). Rather than using the general solution
305 procedure, a more direct way consists of: (i) assuming a value of σ_{cf}; (ii) determining the
306 corresponding values of ε_x, ε_3 and θ from Eqs. (13), using the constitutive relationships of
307 concrete and longitudinal reinforcement; (iii) determining the principal tensile strain using the
308 compatibility condition Eq. (2), i.e. $\varepsilon_1 = \varepsilon_x + (\varepsilon_x - \varepsilon_3)\cot^2\theta$; (iv) calculating the resulting crack
309 opening using Eq. (6); (v) determining the fiber stress corresponding to the obtained crack opening

from Eq. (10); and (vi) iterating through steps (i)-(v) until the resulting fiber effective stress converges with the initially assumed value.

Assuming linear elastic behavior of the concrete in compression and, where applicable, for the longitudinal reinforcement in tension, further simplifications are possible. This is outlined below for two cases of practical interest, representing possible situations in the webs of girders.

Consider first a uniaxially reinforced FRC element loaded in pure shear, i.e. $\rho_z = 0$ and $\sigma_x = \sigma_z = 0$. Using the equilibrium conditions, Eqs. (13), one attains

$$\varepsilon_3 = \varepsilon_{c3} - \frac{n\tau_{zx}^{\ 2}}{\sigma_{cf} E_s}, \qquad \varepsilon_x = \frac{\tau_{zx}}{\rho_x E_s}\left(\frac{\tau_{zx}}{\sigma_{cf}} - \frac{\sigma_{cf}}{\tau_{zx}}\right) \tag{14}$$

and inserting Eqs. (14) into the compatibility condition given by Eq. (2), i.e. $\varepsilon_1 = \varepsilon_x + (\varepsilon_x - \varepsilon_3)\cot^2\theta$, the principal tensile strain amounts to

$$\varepsilon_1 = \frac{\tau_{zx}^{\ 2}}{\rho_x E_s \sigma_{cf}}\left(\frac{\tau_{zx}^{\ 2}}{\sigma_{cf}^{\ 2}}(1 + n\rho_x) - \frac{\sigma_{cf}^{\ 2}}{\tau_{zx}^{\ 2}}\right) \tag{15}$$

Hence, the crack opening $w_r = s_r \varepsilon_1$ (see Eq. (6)) can be expressed in a closed form, and the states of stress and strain are found by simply solving the equation

$$\sigma_{cf}\left(s_{rf} \cdot \frac{\tau_{zx}^{\ 2}}{\rho_x E_s \sigma_{cfi}}\left(\frac{\tau_{zx}^{\ 2}}{\sigma_{cfi}^{\ 2}}(1 + n\rho_x) - \frac{\sigma_{cfi}^{\ 2}}{\tau_{zx}^{\ 2}}\right)\right) = \sigma_{cfi} \tag{16}$$

for an initially assumed value σ_{cfi} of the fiber stress, using $\sigma_{cf}(u)$ defined by Eq. (10) (or any other, more refined FRC constitutive model[42,43]).

Consider next an element with $\rho_x = \rho_z = 0$ of the web of a girder with stiff chords, whose strains are typically dominated by bending moments, but generally also depend on the applied shear stresses, $\varepsilon_x = g(\tau_{zx})$. The equilibrium conditions, Eqs. (13), in this case yield the strains

$$\varepsilon_3 = \varepsilon_{c3} - \frac{n \cdot \tau_{zx}^{\ 2}}{\sigma_{cf} E_s}, \qquad \varepsilon_x = g(\tau_{zx}) \tag{17}$$

and inserting Eqs. (17) into the compatibility condition Eq. (2), i.e. $\varepsilon_1 = \varepsilon_x + (\varepsilon_x - \varepsilon_3)\cot^2\theta$, the principal tensile strain amounts to

$$\varepsilon_1 = g\left(\tau_{zx}\right)\left(1+\frac{\tau_{zx}^{\,2}}{\sigma_{cf}^{\,2}}\right)+\frac{n\tau_{zx}^{\,4}}{E_s\sigma_{cf}^{\,3}} \tag{18}$$

The crack opening $w_r = s_r\varepsilon_1$ (see Eq. (6)) can again be expressed in closed form, and the states of stress and strain are determined by solving the equation

$$\sigma_{cf}\left(s_{rf}\cdot\left(g\left(\tau_{zx}\right)\left(1+\frac{\tau_{zx}^{\,2}}{\sigma_{cfi}^{\,2}}\right)+\frac{n\tau_{zx}^{\,4}}{E_s\sigma_{cfi}^{\,3}}\right)\right)=\sigma_{cfi} \tag{19}$$

for an initially assumed value σ_{cfi}, as above.

DISCUSSION

Figures 5 and 6 present the results of sample compression field analyses for the two special cases discussed above, i.e. a uniaxially reinforced element (Fig. 5) and a FRC element without any conventional reinforcement, but subjected to imposed horizontal strains (Fig. 6), respectively. Two sets of calculations, both considering elastic behavior of the reinforcement, were carried out for each case, i.e. Figs. 5 and 6, considering (i) linear elastic behavior of the concrete, i.e. simply solving Eqs. (16) and (19), respectively, with $n = E_s / E_c = 6$ (dashed lines), and (ii) following the simplified approach for FRC webs outlined in the previous section, using the following parabolic stress-strain relationship accounting for compression softening for the concrete (solid lines)[23,24]:

$$\sigma_{c3} = -\left(\frac{2\varepsilon_{c3}}{\varepsilon_{c0}}-\left(\frac{\varepsilon_{c3}}{\varepsilon_{c0}}\right)^2\right)\frac{f_c^{\,2/3}}{0.4+30\varepsilon_1} \quad \text{i.e.} \quad \varepsilon_{c3} = \varepsilon_{c0}\left(1-\sqrt{1+\frac{\sigma_{c3}}{f_c^{\,2/3}}\left(0.4+30\varepsilon_1\right)}\right) \tag{20}$$

In Eq. (20) f_c is the concrete cylinder strength in MPa and ε_{c0} is the strain corresponding to the peak compressive stress $f_{cred} = f_c^{\,2/3}/\left(0.4+30\varepsilon_1\right)$, with $\varepsilon_{c3} \geq \varepsilon_{c0} \approx -0.002$. The behavior is analyzed for a fiber effectiveness equivalent to $\sigma_{cf\,0} = 2.0\,\text{MPa}$ (0.29 ksi), for both the maximum, as well as the minimum theoretically predicted crack spacing, i.e. $\lambda = 1.0$ and $\lambda = 0.5$, respectively, to study the influence on the response. Furthermore, it is assumed that the fiber geometry and matrix strength are tuned such that ruptures of the fibers do not occur. The considered fiber effectiveness translates to a

steel fiber dosage of approximately 40…60 kg/m^3 (2.5…3.8 lb/ft^3) ($\rho_f = 0.50 - 0.75\%$ by volume) depending on the fiber orientation and the specific properties of the matrix and fibers).

The response of the uniaxially reinforced FRC element in pure shear, $\sigma_x = 0$, is presented in Fig. 5, for a longitudinal reinforcement ratio of $\rho_x = 1.5\%$. The material parameters used in the analyses are indicated in the Figure. It can be seen that as predicted by the second equation in Eq. (13), the principal compressive stress direction rotates towards the horizontal *x*-axis with increasing shear stresses τ_{zx}, and that $\cot\theta$ increases almost proportionally with τ_{zx} as long as the decrease in fiber stresses $\sigma_{c1} = \sigma_{cf}$ due to crack opening *u* is moderate. In the case of *linear elastic* concrete behavior (dashed lines), maximum loads of $\tau_{zxu}/\sigma_{cf0} = 1.63$ and $\tau_{zxu}/\sigma_{cf0} = 1.93$ are predicted for $\lambda = 1.0$ and $\lambda = 0.5$, respectively, with strains in the longitudinal reinforcement reaching $1.77 \cdot 10^{-3}$ and $2.81 \cdot 10^{-3}$. Hence, in this case, depending on the yield strength of the reinforcement, yielding of the reinforcement would govern failure, as indicated by the intersections of the vertical dotted line and model resultants shown in Figs. 5a and 5b for a yield strength of 500 MPa (72.5 ksi). Note that while in an orthogonally reinforced panel, a load increase is possible after yielding of the reinforcement in one direction (accompanied by higher steel stresses in the other reinforcement direction), such a redistribution is not possible in a uniaxially reinforced FRC panel due to the strain-softening characteristics of the FRC. If the yield strength of the reinforcement is sufficiently high, fiber softening would be the governing mode of failure: as the tensile strains, $\varepsilon_1 = \varepsilon_x + (\varepsilon_x - \varepsilon_3)\cot^2\theta$, increase essentially in proportion with $\cot^2\theta$ and hence, with τ_{zx}^2, see the second equation in Eq. (13) , these increasing strains lead to progressively larger crack openings and consequently the ability of the fibers to transmit tension across cracks is reduced, which in turn requires flatter inclinations until the point where equilibrium cannot be satisfied. For *nonlinear* concrete behavior (solid lines), maximum loads of $\tau_{zxu}/\sigma_{cf0} = 1.58$ and $\tau_{zxu}/\sigma_{cf0} = 1.82$ are predicted for $\lambda = 1.0$ and $\lambda = 0.5$, respectively, with corresponding strains at the peak load in the longitudinal reinforcement reaching

$1.56 \cdot 10^{-3}$ and $2.19 \cdot 10^{-3}$. Hence, in this case, reinforcement yielding will not govern unless low strength reinforcement is used and failure occurs when equilibrium cannot be satisfied due to the combined effect of tensile softening of the fiber stresses, as outlined for the linear case, and compression softening of the concrete. The latter is very pronounced, since the compressive strength decreases hyperbolically with increasing tensile strains, ε_1, see Eq. (20) that in turn grow essentially in proportion with $\cot^2\theta$ and τ_{zx}^2, see above, just like the concrete compressive stresses, see the third equation in Eq. (13).

Noting that cracking under pure shear is expected to occur at $\tau_{zxr} = f_{ct} \approx 0.3 f_c^{2/3} = 3.5\,\text{MPa}$ (0.51 ksi), i.e. $\tau_{zxr}/\sigma_{cf0} \approx 1.75$ (or lower if restraint stresses due to shrinkage and hydration heat are considered), it is seen that in spite of the moderate fiber dosage used, with $\sigma_{cf0} < f_{ct}$, the applied shear stresses τ_{zx} can increase after cracking if the crack spacing is small (near the minimum theoretical crack spacing) with $\tau_{zxu}/\tau_{zxr} \approx (1.82 \ldots 1.93)/1.75 = 1.04 \ldots 1.10$, but a brittle failure at cracking would occur for the maximum theoretical crack spacing, with $\tau_{zxu}/\tau_{zxr} \approx (1.58 \ldots 1.63)/1.75 = 0.90 \ldots 0.93$.

By examining the differences between $\lambda = 1.0$ and $\lambda = 0.5$ in Fig. 5, it is evident that the crack spacing has a pronounced effect on the overall behavior, with differences in predicted ultimate loads ranging between 15…20%, even if the specimen is precracked, or if the cracking load is lower than estimated above. Hence, the inherent uncertainty in the spacing of cracks must be acknowledged when analyzing and designing FRC elements subjected to shear. However, even with larger crack spacings, a strain hardening behavior could be obtained using a higher conventional reinforcement ratio, as in the experiments discussed in the following section.

Figure 6 presents the results of a similar analysis for the FRC element without any conventional reinforcement, but subjected to imposed horizontal strains. The material parameters used in the analysis are indicated in the Figure. Horizontal strains were chosen to represent a typical prestressed concrete girder, with an initial prestress of –5 MPa (0.72 ksi) (corresponding to $\varepsilon_x = -0.17 \cdot 10^{-3}$) and

longitudinal strains increasing only slightly until decompression of the tension chord ($\varepsilon_{x,TC} = 0$), which is assumed to occur at $\tau_{zx} = 1.5\,\text{MPa}$ (0.22 ksi). After decompression, longitudinal strains grow faster until the tension chord yields at $\varepsilon_{x,TC} = 2.0 \cdot 10^{-3}$ (e.g. reinforcement with $f_y = 500\,\text{MPa}$ (72.5 ksi) and moderate tension stiffening effect), assumed in the example to occur at $\tau_{zx} = 4\,\text{MPa}$ (0.58 ksi). As usual in design approaches for conventionally reinforced girders, longitudinal strains at the mid-depth of the web are used as a reference point to predict the overall response[19], i.e., neglecting favorable strains of the compression chord, half the longitudinal strains of the tension chord are imposed to the web, $\varepsilon_x = \varepsilon_{x,TC}/2$. Assuming a maximum spacing of the cracks in the tension chord triggering cracks in the web of $s_{r0,TC} = 400\,\text{mm}$ (15.75 in.) and a principal compressive stress direction at cracking of $\theta = 30°$ (a value lower than 45° due to the effect of prestressing), a maximum diagonal crack spacing of $s_{rf0} = 200\,\text{mm}$ (7.87 in.) is obtained from Eq. (9). Since strains are small before cracking of the concrete, which is expected to occur at $\varepsilon_1 = \varepsilon_{ct} = f_{ct}/E_c \approx 10^{-4}$, the cracking load τ_{zxr} is estimated as the shear stress τ_{zxr} acting at $\varepsilon_x = \varepsilon_{ct}$, corresponding to $\tau_{zxr}/\sigma_{cf0} \approx 0.80$ here. Note that in a practical case, all the values assumed above would be determined based on the actual applied prestressing (stress state in web before cracking), the moment-shear interaction at the critical cross-section *M*/*V*, and the tension chord reinforcement layout, using a sectional analysis.

The resulting behavior of the web is generally similar as in the uniaxially reinforced case. Failure is caused by combined tensile softening of the fibers and compression softening of the concrete in all cases. For linear elastic concrete, maximum loads amount to $\tau_{zxu}/\sigma_{cf0} = 2.34$ and $\tau_{zxu}/\sigma_{cf0} = 2.85$ for $\lambda = 1.0$ and $\lambda = 0.5$, respectively. Corresponding values from the nonlinear analysis are $\tau_{zxu}/\sigma_{cf0} = 2.03$ and $\tau_{zxu}/\sigma_{cf0} = 2.21$. Hence, the assumed shear stress in the web at the onset of yielding in the tension chord ($\tau_{zx} = 4\,\text{MPa}$ (0.58 ksi)) is attained in all cases, though with little margin.

Compared to the uniaxially reinforced case, the influence of crack spacing is similar, but somewhat reduced in the nonlinear case (difference on the maximum load about 10%). It can be seen that the deformation capacity is larger, and the increase of shear stresses from cracking to maximum load is substantially more pronounced for the case of where horizontal strains are imposed, with ratios $\tau_{zxu}/\tau_{zxr} \approx (2.03\ldots2.85)/0.8 = 2.54\ldots3.56$, leading to a strain-hardening behavior even in the case of large crack spacings (or if web cracking would occur at much higher loads than assumed here) in spite of $\sigma_{cf0} < f_{ct}$. This indicates that FRC webs without conventional reinforcement should exhibit a much better performance than observed in tests on uniaxially reinforced panels, as long as the chords do not yield; however, this presumption lacks experimental validation as no direct experimental comparison currently exists.

Note that substantial compressive longitudinal stresses ($-\Delta\sigma_x$, see Fig. 4c) are obtained due to the longitudinal restraint caused by the imposed strains; these stresses assume the role of the longitudinal reinforcement and must be resisted by the chords, in addition to chord forces induced by bending (similar to the tension shift in girders with transverse reinforcement).

COMPARISON WITH EXPERIMENTS

In this section, predictions obtained from the simplified compression field analysis for uniaxially reinforced FRC elements outlined above are validated against experimental results of tests carried out by Susetyo et al.[13,48]. In these studies, eight uniaxially reinforced FRC panels ($\rho_x = 3.31\%$, $Ø_x = 8.1\,\text{mm}$ (0.32 in.), $f_s = 552\,\text{MPa}$ (80.1 ksi)) and two orthogonally reinforced reference panels measuring 890×890×70 mm (35×35×3.54 in.) thick were subjected to in-plane shear[29]. Two types of concrete (normal and high strength) and three types of hooked-end fibers, with three different fiber dosages were used. The fiber and matrix characteristics of the FRC panels are given in Table 1; it can be seen that most specimens were provided with unpractically high fiber dosages ($\rho_f = 1.5\%$), reflecting the demands of codes mentioned in the introduction.

448 For all predictions, the fiber stresses are strictly determined using Pfyl's model[3] with
449 $\tau_{bf} = 2 f_{ct} = 0.6 f_c^{2/3}$ (in MPa units) and $K_f = 0.375$, without using any modifications or adaptations
450 based on material tests. Furthermore, the predicted crack spacing is determined from Eq. (8). Except
451 for the test specimens with the lowest fiber dosage, the lower bound $s_r = l_f$ in Eq. (8) governs
452 regardless of the considered value of λ. Therefore, in the following analyses, the crack spacing is
453 not varied (i.e. $\lambda = 1$ is considered). For interest, crack spacings observed in the experiments for fiber
454 dosages of 1.00% and 1.50% match fairly well with $s_r = l_f$, as shown in Table 2.

455 Figure 7 compares predictions carried out assuming (i) linear elastic behavior of the concrete in
456 compression as well as (ii) using the parabolic stress-strain relationship, (see Eq. (20)), to describe
457 the concrete in compression with the experimental results of three tests using normal strength concrete
458 with identical fibers, but with variable fiber dosages (i.e. specimens C1F1V1, C1F1V2, C1F1V3).
459 Both models shown in Fig. 7 consider linear elastic reinforcement behavior. While qualitatively the
460 agreement is satisfactory, the maximum loads and deformations are overestimated, particularly when
461 modelling the concrete as linear elastic, where failure is predicted by yielding of the reinforcement.
462 Note that specimen C1F1V1, with $\rho_f = 0.5\%$, remained uncracked during testing until just prior to
463 attaining maximum load, which explains the much stiffer observed behavior compared to the
464 prediction (which only models the post-cracking range). For nonlinear concrete accounting for
465 compression softening, failure is predicted by combined concrete crushing and fiber softening, but
466 deformations are still overestimated (albeit much less than by Reference[48], in spite of their
467 customization of the tension softening characteristics of the FRC for each individual experiment, also
468 shown in Fig. 7). The most plausible explanation is the premature failure of the elements by sliding
469 along cracks generated in early load-stages, as observed in the tests[13]. Such failures, which are
470 difficult to distinguish from concrete crushing in experiments, are not reflected by rotating-crack
471 models like the CMM-Rf. These models implicitly assume that stresses can be transferred across
472 cracks formed at earlier load stages, whose direction may deviate significantly from the principal

473 direction assumed at higher loads. In order to capture this effect, a model considering fixed,
474 interlocked cracks, such as the CMM-F, would be required. Another explanation could be that with
475 the fiber type used in the three experiments illustrated in Fig. 7, the fiber-fracture condition
476 represented by Eq. (12) is exceeded by roughly 25%, such that the fibers with the longest embedded
477 length would fracture, instead of being pulled out as assumed in the predictions. Although the failure
478 surfaces of the panels were not reported by Susetyo, he noted that the panels did not contain any
479 fractured fibers in any of the dominant cracks[13]. However, as fiber-fracture would only affect a small
480 portion of total amount of fibers bridging the crack it can only explain a small part of the
481 overestimation.
482 Figure 8 compares predictions carried out using the parabolic stress-strain relationship to describe the
483 concrete in compression using Eq. (20), with the experimental results of the remaining tests on FRC
484 panels documented in Reference[48], all with identical fiber dosage ($\rho_f = 1.5\%$) but different types of
485 hooked end fibers. Again, the agreement is satisfactory, particularly when compared to those in
486 Reference[48] (shown in Fig. 8), however deformations and maximum loads are overestimated for both
487 the normal strength concrete panels, (refer to Fig. 8a), as well as the high strength concrete specimens
488 shown in Fig. 8b. Possible explanations for the normal strength concrete panels are the same as
489 discussed above. The more pronounced differences in the high strength concrete specimens could be
490 explained by the smoother crack faces in high strength concrete, caused by cracks passing through
491 the aggregates (rather than around them as is the case for normal strength concrete)[49]. Furthermore,
492 in Specimen C2F1V3-R, the fiber-fracture condition given by Eq. (12) is violated by roughly 70%,
493 such that the majority of the fibers in this case would fracture rather than pull out as assumed in the
494 predictions; this could basically explain the overestimation of maximum load as well as deformations.
495 However, similar results are obtained for Specimen C2F2V3, where only about 75% of the tensile
496 strength of the fibers is reached according to Eq. (12). Hence, this explanation does not appear to be
497 conclusive.

For interest, the predicted responses by Lee et al.[50] using a finite element approach are also provided in Figs. 7 and 8. In their model, Lee et al. considered crack slip, which essentially represents a fixed crack model, however, disregarded the interaction between fiber stresses and aggregate interlock in the transfer of shear across cracks. Despite the excellent correlation with the test data, it is questionable whether the semi-empirical approach by Lee is extendable to other, more practical dosages of SFRC.

SUMMARY AND CONCLUSIONS

This paper presents a simplified rotating crack model for the analysis and design of steel fiber reinforced elements in shear (CMM-Rf) based on the Cracked Membrane Model with stress-free cracks (CMM-R)[23,24]. Simplified solution procedures of the CMM-Rf are developed for (i) uniaxially reinforced FRC elements in pure shear and (ii) FRC elements without conventional reinforcement, but with imposed longitudinal strains. It is shown that the applied load can be increased after cracking even when using practical, moderate fiber dosages. This is due to the fact that more fibers can be activated by progressively rotating the principal compressive stress direction towards the direction of the uniaxial reinforcement or imposed strain, respectively. A hardening response is thus obtained until the point where due to the softening of the fibers, excessively flat inclinations of the principal compressive stress direction are required to maintain equilibrium, resulting in failures by concrete crushing particularly if compression softening is accounted for.

The model is compared with available test data and shows a satisfactory correlation. However, it is revealed that rotating crack models are not capable of capturing failures which are governed by sliding of cracks in elements with high fiber dosages. In order to cover such cases, it is proposed to extend the general Cracked Membrane Model (CMM-F)[23,24], which considers interlocked cracks with a fixed orientation, to account for fiber reinforcement, in a future study.

Finally, more experimental data is required in order to validate theoretical models, particularly with practical and economical fiber dosages, as well as to investigate the behavior of FRC elements without any conventional reinforcement, but with imposed longitudinal strains.

REFERENCES

1. Voo, Y. L., Foster, S. J., and Voo, C. C., "Ultrahigh-Performance Concrete Segmental Bridge Technology: Toward Sustainable Bridge Construction," *Journal of Bridge Engineering*, V. 20, No. 8, Aug. 2015, p. B5014001–1:12. doi: 10.1061/(ASCE)BE.1943-5592.0000704
2. Standards Australia. "AS 3600:2018. Australian Standard, Concrete Structures," 2018.
3. Pfyl, T. "Tragverhalten von Stahlfaserbeton." PhD thesis, Institute of Structural Engineering, ETH Zurich, Switzerland, 2003.
4. Dancygier, A. N., and Berkover, E., "Cracking localization and reduced ductility in fiber-reinforced concrete beams with low reinforcement ratios," *Engineering Structures*, V. 111, Mar. 2016, pp. 411–424. doi: 10.1016/j.engstruct.2015.11.046
5. Marti, P., Alvarez, M., Kaufmann, W., and Sigrist, V., "Tension Chord Model for Structural Concrete," *Structural Engineering International*, V. 8, No. 4, Nov. 1998, pp. 287–298. doi: 10.2749/101686698780488875
6. Alvarez, M., and Marti, P. "Versuche zum Verbundverhalten von Bewehrungsstahl bei plastischen Verformungen," v. vol. 222, Birkhäuser, 1996, 135 pp.
7. Sigrist, V., and Marti, P. "Versuche zum Verformungsvermögen von Stahlbetonträgern," v. vol. 202, Zurich, Switzerland, Institute of Structural Engineering, ETH Zurich, 1993, 90 pp.
8. Kaufmann, W., and Marti, P. "Versuche an Stahlbetonträgern unter Normal- und Querkraft," v. vol. 226, Basel, Switzerland, Birkhäuser, 1996.
9. Rupf, M. "Querkraftwiderstand von Stahlbeton- und Spannbetonträgern mittels Spannungsfeldern." PhD thesis, École polytechnique fédérale de Lausanne (EPFL), Switzerland, 2014.
10. Angelakos, D., Bentz, E. C., and Collins, M. P., "Effect of Concrete Strength and Minimum Stirrups on Shear Strength of Large Members," *ACI Structural Journal*, V. 98, No. 3, May 2001, pp. 290–300. doi: 10.14359/10220

549 11. Rahal, K. N., and Al-Shaleh, K. S., "Minimum Transverse Reinforcement in 65 Mpa Concrete
550 Beams," *Structural Journal*, V. 101, No. 6, Nov. 2004, pp. 872–878. doi: 10.14359/13463
551 12. Minelli, F. "Plain and fiber reinforced concrete beams under shear loading: structural behavior
552 and design aspects." PhD thesis, Department of Civil Engineering, University of Brescia, Italy,
553 2005.
554 13. Susetyo, J. "Fibre Reinforcement for Shrinkage Crack Control in Prestressed, Precast Segmental
555 Bridges." PhD thesis, Department of Civil Engineering, University of Toronto, Canada, 2010.
556 14. Adebar, P., Mindess, S., St.-Pierre, D., and Olund, B., "Shear Tests of Fiber Concrete Beams
557 without Stirrups," *ACI Structural Journal*, V. 94, No. 1, Jan. 1997, pp. 68–76. doi: 10.14359/462
558 15. Aoude, H., Belghiti, M., Cook, W. D., and Mitchell, D., "Response of Steel Fiber-Reinforced
559 Concrete Beams with and without Stirrups," *ACI Structural Journal*, V. 109, No. 3, May 2012,
560 pp. 359–368. doi: 10.14359/51683749
561 16. Standards Australia. "AS 5100.5:2017. Bridge design Part 5: Concrete," 2017.
562 17. Standards New Zealand "NZS 3101: Concrete structures standard Part 2 – commentary on the
563 design of concrete structures," Wellington, New Zealand, Standards New Zealand, 2006, 391 pp.
564 18. ACI Committee 318 "Building code requirements for structural concrete (ACI 318-08) and
565 commentary," Farmington Hills, MI, American Concrete Institute, 2009.
566 19. International Federation for Structural Concrete. "fib Model Code for Concrete Structures 2010,"
567 Berlin, Germany, Wilhelm Ernst & Sohn, 2013, 402 pp.
568 20. Bentz, E. C. "MC2010: Shear Strength of Beams and Implications of the New Approaches."
569 Recent Developments on Shear and Punching Shear on RC and FRC Elements. Lausanne,
570 Switzerland, International Federation for Structural Concrete, 2010. pp. 15–30.
571 21. Foster, S. J. "Design of FRC beams for shear using the VEM and the draft model code approach."
572 Recent Developments on Shear and Punching Shear on RC and FRC Elements. Lausanne,
573 Switzerland, International Federation for Structural Concrete, 2010. pp. 15–30.
574 22. European Committee for Standardization "Eurocode 2: Design of concrete structures - Part 1-1:
575 General rules and rules for buildings," n.d.
576 23. Kaufmann, W. "Strength and deformations of structural concrete subjected to in-plane shear and
577 normal forces." PhD thesis, Institute of Structural Engineering, ETH Zurich, Birkhäuser Verlag,
578 Basel, Switzerland, 1998.

579 24. Kaufmann, W., and Marti, P., "Structural Concrete: Cracked Membrane Model," *Journal of*
580 *Structural Engineering, ASCE*, V. 124, Dec. 1998, pp. 1467–1475. doi: 10.1061/(ASCE)0733-
581 9445(1998)124:12(1467)
582 25. Kupfer, H. "Erweiterung der Mörsch'schen Fachwerkanalogie mit Hilfe des Prinzips vom
583 Minimum der Formänderungsenergie," *CEB Bulletin d'information*, No. 40, 1964, pp. 44–57.
584 26. Collins, M. P. "Towards a Rational Theory for RC Members in Shear," *Journal of the Structural*
585 *Division, ASCE*, V. 104, No. 4, 1978, pp. 649–66.
586 27. Baumann, T. "Zur Frage der Netzbewehrung von Flächentragwerken," *Bauingenieur*, V. 47, No.
587 10, 1972, pp. 367–77.
588 28. Mitchell, D., and Collins, M. P., "Diagonal Compression Field theory - A Rational Model For
589 Structural Concrete in Pure Torsion," *ACI Journal*, V. 71, No. 8, Aug. 1974, pp. 396–408. doi:
590 10.14359/7103
591 29. Vecchio, F. J., and Collins, M. P., "The Modified Compression-Field Theory for Reinforced
592 Concrete Elements subjected to Shear," *ACI Journal*, V. 83, No. 2, Mar. 1986, pp. 219–231. doi:
593 10.14359/10416
594 30. Kaufmann, W., Mata-Falcón, J., and Beck, A. "Future directions for research on shear in
595 structural concrete." fib Bulletin 85: Towards a rational understanding of shear in beams and
596 slabs. 2018. pp. 323–38.
597 31. Hsu, T. T. C., "Softened Truss Model Theory for Shear and Torsion," *ACI Structural Journal*,
598 V. 85, No. 6, Nov. 1988, pp. 624–635. doi: 10.14359/2740
599 32. Vecchio, F. J., "Disturbed Stress Field Model for Reinforced Concrete: Formulation," *Journal of*
600 *Structural Engineering, ASCE*, V. 126, No. 9, Sep. 2000, pp. 1070–1077. doi:
601 10.1061/(ASCE)0733-9445(2000)126:9(1070)
602 33. Foster, S. J., and Marti, P., "Cracked Membrane Model: Finite element implementation," *Journal*
603 *of Structural Engineering, ASCE*, V. 129, No. 9, 2003, pp. 1155–1163. doi:
604 10.1061/(ASCE)0733-9445(2003)129:9(1155)
605 34. Pimentel, M., and Figueiras, J. "Model for the analysis of structural concrete elements under
606 plane stress conditions: FE implementation." Computational modelling of Concrete Structures.
607 Austria, CRC Press, 2010. pp. 391–400.

608 35. Thoma, K., Roos, P., and Weber, M., “Finite-Elemente-Analyse von Stahlbetonbauteilen im
609 ebenen Spannungszustand,” *Beton- und Stahlbetonbau*, V. 109, No. 4, 2014, pp. 275–283. doi:
610 doi.org/10.1002/best.201300087
611 36. Seelhofer, H. “Ebener Spannungszustand im Betonbau: Grundlagen und Anwendungen.” PhD
612 thesis, Institute of Structural Engineering, ETH Zurich, vdf Hochschulverlag, Switzerland, 2009.
613 37. Karagiannis, D., and Kaufmann, W. “Capacity Assessment of Concrete Box-Girder Bridge Webs
614 Against the Combined Action of In-plane Shear and Transverse Bending.” In: Hordijk, D. A.,
615 Luković, M., eds. High Tech Concrete: Where Technology and Engineering Meet. Maastricht,
616 The Netherlands, Springer, 2018. pp. 693–700.
617 38. Thoma, K., “Finite element analysis of experimentally tested RC and PC beams using the cracked
618 membrane model,” *Engineering Structures*, V. 167, Jul. 2018, pp. 592–607. doi:
619 10.1016/j.engstruct.2018.04.010
620 39. Kaufmann, W., and Mata-Falcón, J. “Crack Widths in Structural Concrete Subjected to In-Plane
621 Loading.” Workshop Proceedings No. 12. Oslo, Norway, Nordic Concrete Federation, 2017. pp.
622 21–5.
623 40. Marti, P., Pfyl, T., Sigrist, V., and Ulaga, T., “Harmonized Test Procedures for Steel Fiber-
624 Reinforced Concrete,” *ACI Materials Journal*, V. 96, No. 6, Nov. 1999, pp. 676–685. doi:
625 10.14359/794
626 41. Amin, A., Foster, S. J., Gilbert, R. I., and Kaufmann, W., “Material characterisation of macro
627 synthetic fibre reinforced concrete,” *Cement and Concrete Composites*, V. 84, Nov. 2017, pp.
628 124–133. doi: 10.1016/j.cemconcomp.2017.08.018
629 42. Ng, T. S., Htut, T., and Foster, S. “Fracture of Steel Fibre Reinforced Concrete – The Unified
630 Variable Engagement Model,” Sydney, Australia, School of Civil and Environmental
631 Engineering, The University of New South Wales, 2012, 107 pp.
632 43. Lee, S.-C., Cho, J.-Y., and Vecchio, F. J., “Diverse Embedment Model for Steel Fiber-Reinforced
633 Concrete in Tension: Model Development,” *ACI Materials Journal*, V. 108, No. 5, 2011, pp.
634 516–525. doi: 10.14359/51683261
635 44. Foster, S. J., “On Behavior of High-Strength Concrete Columns: Cover Spalling, Steel Fibers,
636 and Ductility,” *ACI Structural Journal*, V. 98, No. 4, Jul. 2001, pp. 583–589. doi:
637 10.14359/10301

638 45. Amin, A., and Foster, S. J. “Shear strength of steel fibre reinforced concrete beams with stirrups,”
639 *Engineering Structures*, V. 111, 2016, pp. 323–32. doi: 10.1016/j.engstruct.2015.12.026
640 46. Deluce, J. R. “Cracking Behaviour of Steel Fibre Reinforced Concrete Containing Conventional
641 Steel Reinforcement.” MSc dissertation, Department of Civil Engineering, University of
642 Toronto, 2011.
643 47. Amin, A. “Post Cracking Behaviour of Steel Fibre Reinforced Concrete: From Material to
644 Structure,” PhD Thesis, School of Civil and Environmental Engineering, The University of New
645 South Wales, 2015.
646 45. Susetyo, J., Gauvreau, P., and Vecchio, F. J., “Steel Fiber-Reinforced Concrete Panels in Shear:
647 Analysis and Modeling,” *ACI Structural Journal*, V. 110, No. 2, Mar. 2013, pp. 285–296. doi:
648 10.14359/51684408
649 49. Walraven, J. C. “Fundamental Analysis of Aggregate Interlock,” *Journal of the Structural*
650 *Division, ASCE*, V. 107, No. 11, 1981, pp. 2245–70.
651 50. Lee, S.-C., Cho, J.-Y., and Vecchio, F. J. “Analysis of Steel Fiber-Reinforced Concrete Elements
652 Subjected to Shear,” *ACI Structural Journal*, V. 113, No. 2, 2016, pp. 275–85.
653

APPENDIX

This Appendix contains additional information that were not provided in the main body of the paper for the sake of brevity.

Notation

d_f	=	diameter of fiber
E_c	=	elastic modulus of concrete
E_f	=	elastic modulus of fibers
E_s	=	elastic modulus of steel reinforcement
E_{sh}	=	hardening modulus of steel reinforcement
K_f	=	fiber orientation factor
f_c	=	compressive strength of concrete matrix
f_{ct}	=	tensile strength of concrete matrix
f_s	=	yield strength of longitudinal reinforcement
f_t	=	ultimate strength of longitudinal reinforcement
f_{tf}	=	ultimate strength of fiber reinforcement
l_f	=	length of fiber
l_{fb}	=	embedded length of fiber
n	=	modular ratio
s_r	=	diagonal crack spacing without fibres
s_{r0}	=	maximum diagonal crack spacing without fibres
s_{rf}	=	diagonal crack spacing for SFRC members
s_{rf0}	=	maximum diagonal crack spacing for SFRC members
u	=	orthogonal crack opening
V_R	=	total shear force
V_{Rc}	=	ultimate shear force carried by concrete
V_{Rf}	=	ultimate shear force carried by fibers
V_{Rs}	=	ultimate shear force carried by transverse reinforcement
w_r	=	crack opening
ε	=	strain
ε_{c0}	=	strain of concrete corresponding to the peak compressive stress
ε_{su}	=	ultimate tensile strain of longitudinal reinforcement

685 γ_{zx} = shear strain

686 λ = crack spacing coefficient

687 σ_c = stress in concrete

688 σ_{cf} = effective (residual) fiber stresses at the cracks

689 σ_s = stress in steel reinforcement

690 ρ_f = volumetric fiber dosage

691 $\rho_{f,\min}$ = minimum volumetric fiber dosage for SFRC members

692 $\rho_{\min}$ = minimum longitudinal reinforcing ratio

693 ρ_x = longitudinal reinforcing ratio in *x*-direction

694 ρ_z = longitudinal reinforcing ratio in *z*-direction

695 τ_b = bond shear stress for reinforcing bar and matrix

696 τ_{bf} = bond shear stress for fiber and matrix

697 τ_{zx} = applied shear stress

698 θ = principal compressive stress and strain direction

699 θ_f = fiber inclination

700 θ_r = crack direction

701 $\varnothing$ = steel reinforcing bar diameter

702

703 **Calculation of fiber orientation factor**

704 Assuming that all possible fiber orientations have an equal probability of occurrence (either in 2D or

705 3D, or, in few cases, in-between), the fiber orientation factor, K_f, is obtained by integrating all

706 possible fiber orientations, observing that the amount of fibers with an inclination θ_f crossing a crack

707 plane of unit surface amounts to $\cos\theta_f$, see Fig. A.1a. Discounting the fibers whose inclination

708 exceeds $|\theta_f| > \theta_{eff}$, one obtains

709 $$K_f = \frac{1}{\pi}\int_{-\theta_{eff}}^{\theta_{eff}} \cos\theta_f d\theta_f = \frac{2}{\pi}\sin\theta_{eff} \quad \left(\theta_{eff} = \frac{\pi}{2}:\ K_f = \frac{2}{\pi};\quad \theta_{eff} = \frac{\pi}{3}:\ K_f = \frac{\sqrt{3}}{\pi}\right) \qquad (A.1)$$

710 for a 2D fiber distribution and

$$K_f = \frac{1}{2\pi}\int_{-\pi}^{\pi}\int_{0}^{\theta_{eff}} \cos\theta_f \, dA = \frac{1}{2}\sin^2\theta_{eff} \quad \left(\theta_{eff} = \frac{\pi}{2}:\ K_f = \frac{1}{2};\quad \theta_{eff} = \frac{\pi}{3}:\ K_f = \frac{3}{8}\right) \tag{A.2}$$

for a 3D fiber distribution, where $dA = \sin\theta_f \cdot d\theta_f \cdot d\varphi$ in spherical coordinates has been used.

Note that Eqs. (A.1) and (A.2) can be interpreted as the projection of the surface S defined by the fiber end loci of all effective fibers to the crack plane (a semi-circle and a semi-sphere for the 2D and 3D case), divided by the surface S, see Fig. A.1b and c, respectively.

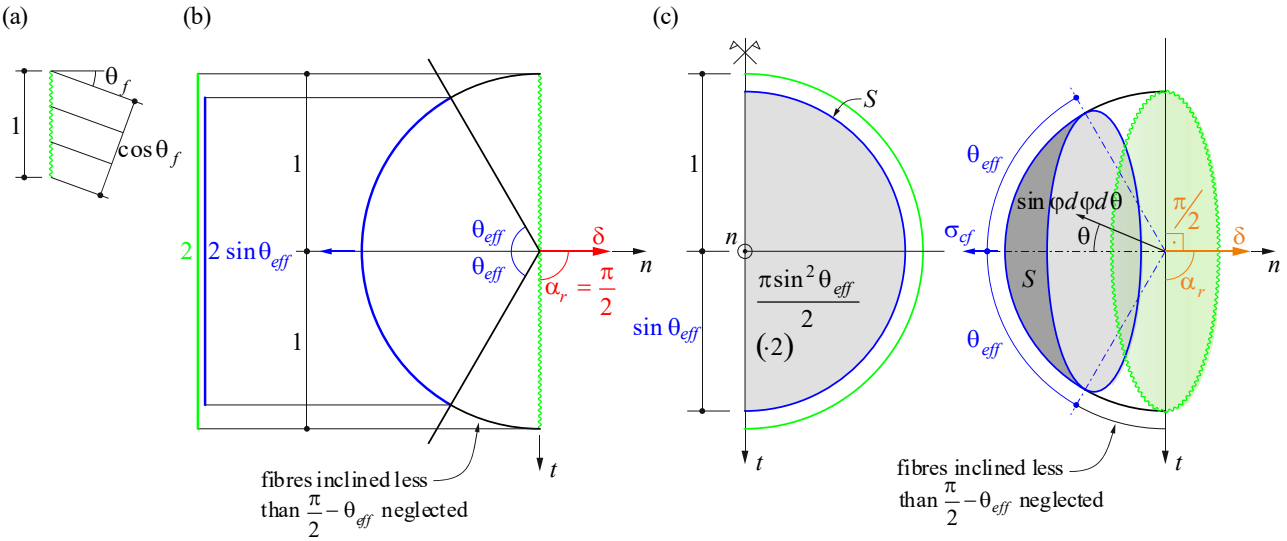

Fig. A.1– Fiber orientation factor for orthogonal crack opening: (a) notation, (b) 2D and (c) 3D fiber distribution, respectively, neglecting fibers oriented close to the crack plane.

TABLES AND FIGURES

List of Tables:

List of Figures:

744 Fig. 6 – FRC element without conventional reinforcement, but imposed horizontal strains,
745 comparison of simplified linear (dashed lines) and nonlinear (solid lines) compression field analysis
746 with increasing shear τ_{zx} for maximum and minimum theoretical crack spacing: (a) Normalized fiber
747 stresses σ_{cf}/σ_{cf0} and concrete compressive stresses $-\sigma_{c3}/f_{cred}$, $-\sigma_{c3}/f_c$; (b) principal direction
748 $\cot\theta$ [-], crack opening u [mm], longitudinal strains ε_x [-], and shear strains γ_{zx}.
749 Fig. 7 – Comparison of predictions by the simplified compression field with tests by Susetyo et al.[48]
750 for nonlinear concrete, accounting for compression softening (solid lines) and linear elastic concrete
751 (dashed lines). For comparison, predictions given in in References[48,50] are also indicated.
752 Fig. 8 – Comparison of predictions by the simplified compression field with tests by Susetyo et al.[48]
753 for nonlinear concrete, accounting for compression softening: (a) normal strength concrete; (b) high
754 strength concrete. For comparison, predictions given in References[48,50] are also indicated.
755

Table 1 – Fiber and matrix characteristics of tests by Susetyo et al.[48] (specimen designation: C=concrete type 1-2; F=fiber type 1-3; V=fiber dosage 1-3; R=repeated due to experimental problems in initial test).

Specimen	f_c [MPa] ([ksi])	$-\varepsilon_{c0}$ ($x10^{-3}$)	ρ_f (%)	d_f [mm] ([in.])	l_f [mm] [(in.)]	f_{tf} [MPa] [(ksi)]
C1F1V1	51.4 (7.45)	2.15	0.50	0.62 (0.024)	50 (1.97)	1050 (152.3)
C1F1V2	53.4 (7.74)	2.67	1.00	0.62 (0.024)	50 (1.97)	1050 (152.3)
C1F1V3	49.7 (7.21)	2.50	1.50	0.62 (0.024)	50 (1.97)	1050 (152.3)
C1F2V3	59.7 (8.66)	3.27	1.50	0.38 (0.015)	30 (1.18)	2300 (333.6)
C1F3V3	45.5 (6.60)	2.34	1.50	0.55 (0.022)	35 (1.38)	1100 (159.5)
C2F1V3-R	78.8 (11.43)	2.78	1.50	0.62 (0.024)	50 (1.97)	1050 (152.3)
C2F2V3	76.5 (11.10)	2.22	1.50	0.38 (0.015)	30 (1.18)	2300 (333.6)
C2F3V3	62.0 (8.99)	2.03	1.50	0.55 (0.022)	35 (1.38)	1100 (159.5)

Table 2 – Comparison of predicted crack spacing, s_{rf}, and observed average crack spacing, $s_{r,exp}$, for tests by Susetyo et al.[48].

Specimen	$s_{r,exp}$ [mm] ([in.])	s_{rf} (λ=0.5) - Eq. (8) [mm] ([in.])	s_{rf} (λ=1.0) - Eq. (8) [mm] ([in.])
C1F1V1	114 (4.49)	146 (5.75)	73 (2.87)
C1F1V2	55 (2.17)	50 (1.97)	50 (1.97)
C1F1V3	57 (2.24)	50 (1.97)	50 (1.97)
C1F2V3	38 (1.50)	30 (1.18)	30 (1.18)
C1F3V3	57 (2.24)	35 (1.38)	35 (1.38)
C2F1V3-R	36 (1.42)	50 (1.97)	50 (1.97)
C2F2V3	47 (1.85)	30 (1.18)	30 (1.18)
C2F3V3	41 (1.61)	35 (1.38)	35 (1.38)

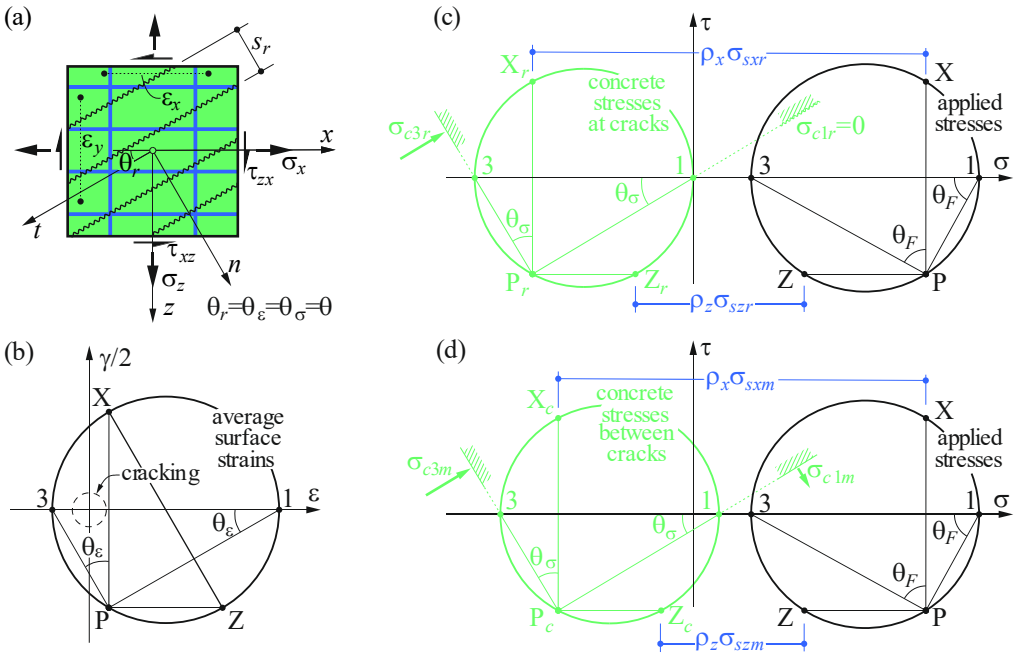

764

765 *Fig. 1 – Compression field approaches: (a) notation; (b) average surface strains; (c) concrete*
766 *stresses at cracks (zero tensile stresses in the concrete); (d) concrete stresses (including tensile*
767 *stresses in the concrete).*

768

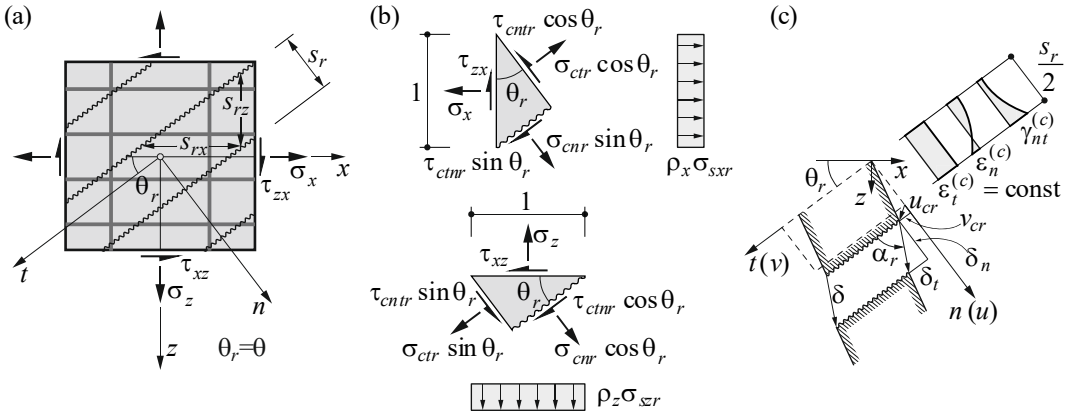

769

770 *Fig. 2 – Cracked membrane element with one set of parallel cracks of fixed direction: (a) element*
771 *with applied stresses; (b) stresses at the crack; (c) crack kinematics.*

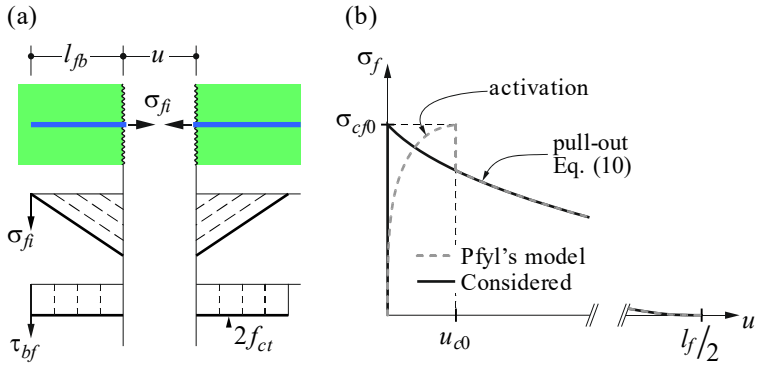

Fig. 3 – Fiber engagement at orthogonal crack openings: (a) Single fiber pullout; (b) FRC activation and pullout phases.

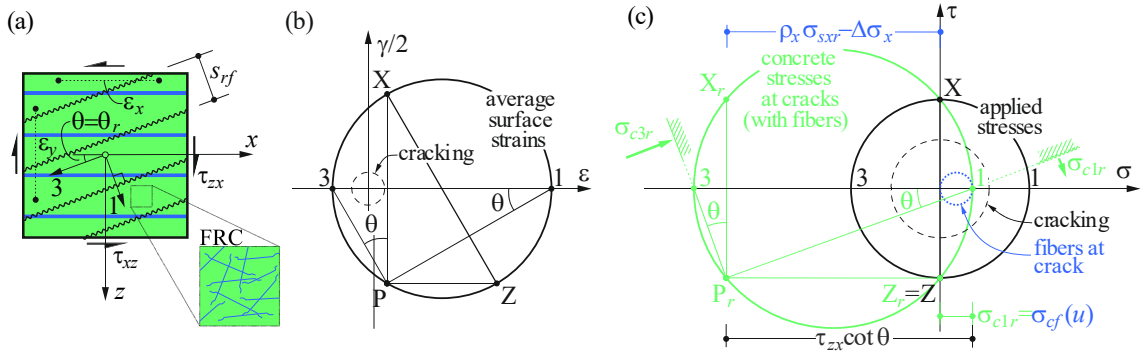

Fig. 4 – Compression field approach for FRC element with $\rho_z = 0$, $\sigma_z = 0$: (a) notation; (b) average surface strains; (c) stresses at cracks.

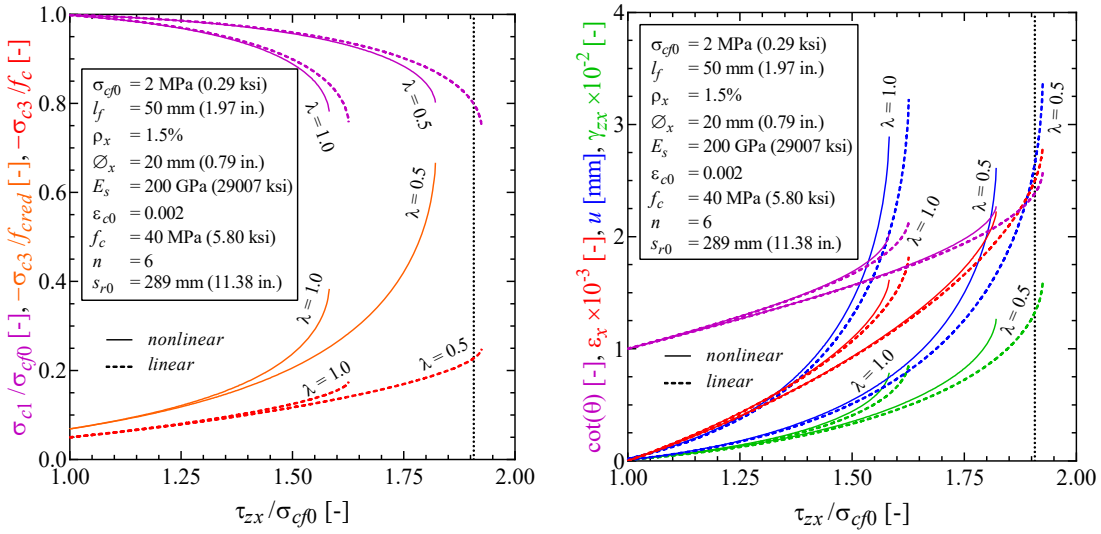

781 *Fig. 5 – Uniaxially reinforced FRC element in pure shear, comparison of simplified linear (dashed*
782 *lines) and nonlinear (solid lines) compression field analysis with increasing shear* τ_{zx} *for maximum*
783 *and minimum theoretical crack spacing: (a) Normalized fiber stresses* σ_{cf}/σ_{cf0} *and concrete*
784 *compressive stresses* $-\sigma_{c3}/f_{cred}$ *,* $-\sigma_{c3}/f_c$ *; (b) principal direction* $\cot\theta$ *[-], crack opening u [mm],*
785 *longitudinal strains* ε_x *[-], and shear strains* γ_{zx} *[-](vertical dotted lines indicate yielding of a 500*
786 *MPa yield strength reinforcement).*

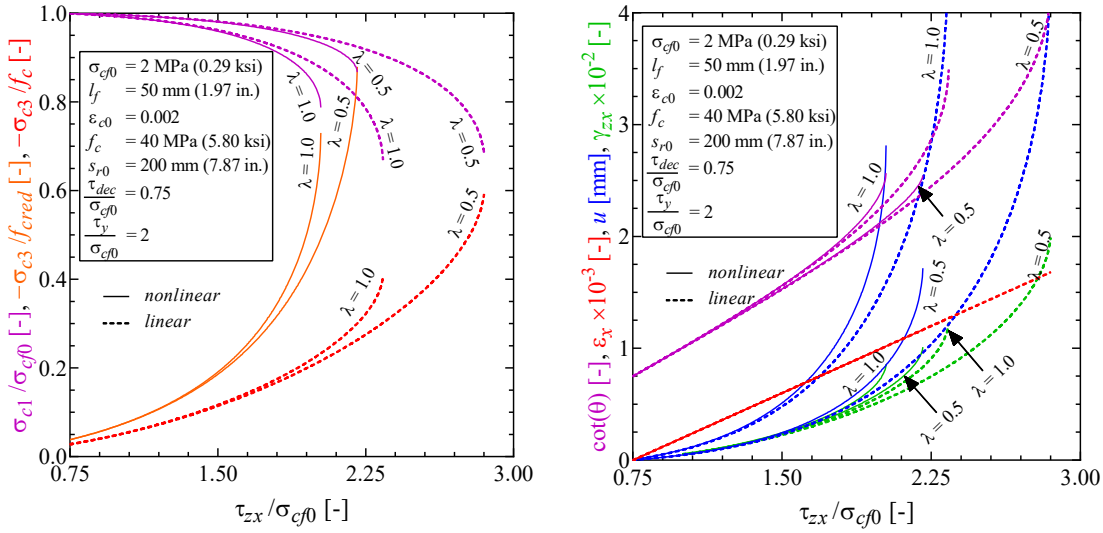

787 *Fig. 6 – FRC element without conventional reinforcement, but imposed horizontal strains,*
788 *comparison of simplified linear (dashed lines) and nonlinear (solid lines) compression field analysis*
789 *with increasing shear* τ_{zx} *for maximum and minimum theoretical crack spacing: (a) Normalized fiber*
790 *stresses* σ_{cf}/σ_{cf0} *and concrete compressive stresses* $-\sigma_{c3}/f_{cred}$ *,* $-\sigma_{c3}/f_c$ *; (b) principal direction*
791 $\cot\theta$ *[-], crack opening u [mm], longitudinal strains* ε_x *[-], and shear strains* γ_{zx}*.*

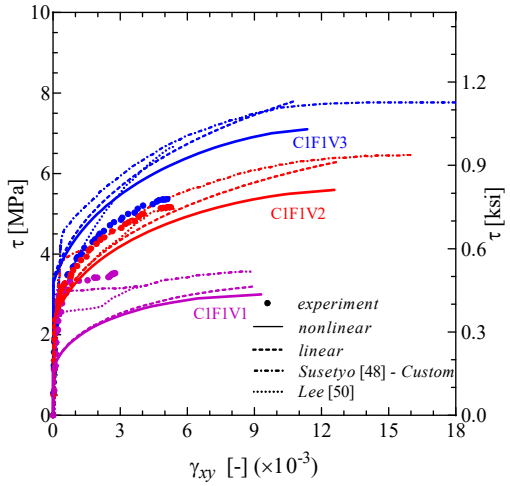

792

793 *Fig. 7 – Comparison of predictions by the simplified compression field with tests by Susetyo et al.*[48]
794 *for nonlinear concrete, accounting for compression softening (solid lines) and linear elastic concrete*
795 *(dashed lines). For comparison, predictions given in in References*[48,50] *are also indicated.*

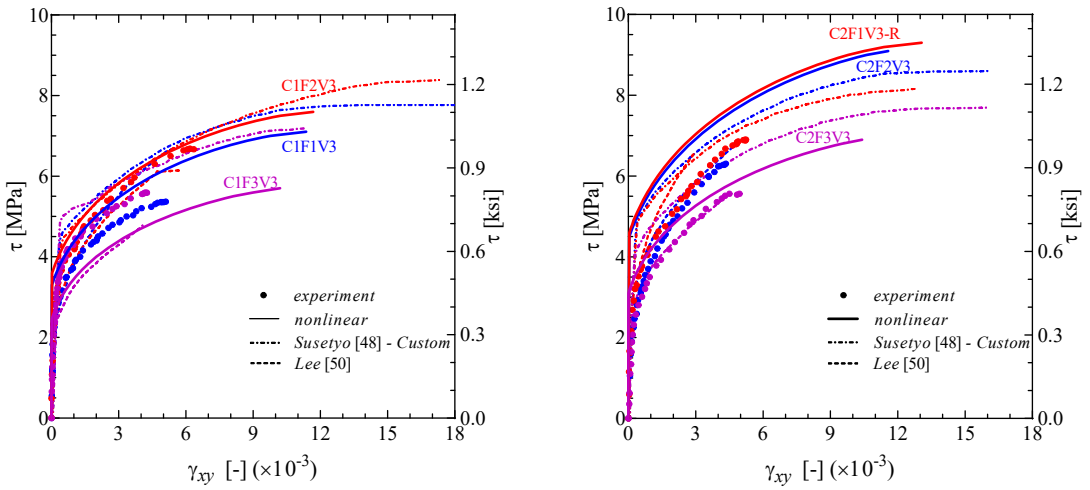

796 *Fig. 8 – Comparison of predictions by the simplified compression field with tests by Susetyo et al.*[48]
797 *for nonlinear concrete, accounting for compression softening: (a) normal strength concrete; (b) high*
798 *strength concrete. For comparison, predictions given in References*[48,50] *are also indicated.*